Article:

Ma, W, Wang, H, Wang, Y orcid.org/0000-0002-5673-042X et al. (2 more authors) (2022) Experimental and simulation studies of the effect of surface roughness on corrosion behaviour of X65 carbon steel under intermittent oil/water wetting. Corrosion Science, 195. 109947. ISSN 0010-938X

https://doi.org/10.1016/j.corsci.2021.109947

Experimental and simulation studies of the effect of surface roughness on corrosion behaviour of X65 carbon steel under intermittent oil/water wetting

Wenlong Ma[a,c], Hanxiang Wang[a], Yongxing Wang[d], Anne Neville[c] and Yong Hua[b]**

[a] College of Mechanical and Electrical engineering, China University of Petroleum (East China), Qingdao, 266555, China

[b] School of Materials Science and Engineering, China University of Petroleum (East China), Qingdao, China

[c] School of Mechanical Engineering, University of Leeds, Leeds, LS2 9JT, United Kingdom

[d] School of Computing, University of Leeds, Leeds, LS2 9JT, United Kingdom

**Corresponding authors:*
Yong Hua: leo.huayong@gmail.com;
Hanxiang Wang: wanghx1899@163.com

Abstract:

The effect of surface roughness on corrosion behaviour of carbon steel under intermittent oil/water wetting with different flow conditions was investigated by an "alternate wetting cell", combining with potentiostatic polarisation, contact angle measurement, and computational fluidic dynamics (CFD) analysis. Under static flow conditions, the rough surface increased the oil film lifetime and consequently mitigated the corrosion as the oil film has good adhesion and acted as a blocking barrier. However, under dynamic flow conditions, the smooth surface of 6 Micron shows the longest oil film lifetime and highest corrosion mitigation efficiency, caused by small turbulence eddies and low shear stress.

Keywords: *Carbon steel, CO_2 corrosion, Surface Roughness, CFD, Intermittent oil/water wetting*

1. Introduction

In the oil and gas industry, the safe and efficient transportation of hydrocarbons via transmission pipelines is important to achieve the greatest value from the extraction of oil reservoirs [1]. To maximize flow efficiency and prolong life, the optimization design of pipelines has been widely implemented in the petroleum industry. Surface roughness is a vital design parameter that influences the flow efficiency through the pressure and energy loss caused by friction [2]. In engineering, the optimized surface roughness is often determined by the Moody diagram, which relates friction factor to Reynolds number for different roughness under various flow conditions. Meanwhile, surface roughness also influences corrosion, a significant factor determining the working lifetime of pipelines. Therefore, investigating the effect of surface roughness on corrosion behaviour under various working conditions can contribute to a better design of pipelines.

Under static or laminar flow conditions, a rough surface not only increased the general corrosion rate [3-8] but also accentuated the pitting corrosion [3-4]. Previous research has attributed the above phenomenon to the effect of surface roughness on surface electron work function (EWF), representing the minimum energy to remove an electron from the metal surface [3, 5, 8]. The average EWF of a rough surface was low, therefore, a high corrosion rate was recorded [3-6] and the corrosion inhibitor was hard to be adsorbed on the surface [7-8]. Besides, fluctuation of local EWF increased with surface roughness, promoting the formation of the microelectrode and inducing the pitting corrosion on the surface [3-5].

Under turbulent flow conditions, the corrosion rate increased with surface roughness due to the near-wall flow characteristics around steel surface [8-10]. In the near-wall flow, large turbulence eddies induced by the rough surface accelerating the mass transfer and corrosion process [11-12]. Besides, Evgeny et al. [8] pointed out that turbulent eddies in cavities of the rough surface could erode the inhibitor film and decrease its adsorption stability. The previous research [3-10] gave a good insight into the effect of surface roughness on corrosion behaviour in a single-phase flow, however, rare research has been conducted in an oil/water flow.

Compared with water-wetting and oil-wetting states, the intermittent oil/water wetting state complicates the corrosion process of oil/water transmission pipelines [13-15]. Schmitt et al. [13] found that high-frequency wetting cycles accelerated the localized corrosion of carbon steel near the oil/water interface. Wang et al. [14] revealed that low flow velocity and high wetting frequency mitigated the general corrosion of carbon steel. Tang [15] pointed out that the static contact angle for the rough surface couldn’t accurately reflect the actual wettability of that under low-frequency dynamic wetting. Despite the above contribution to further understanding the corrosion behaviour of carbon steel under intermittent wetting, the effect of surface roughness under such working conditions was still unclear. Besides, the corrosion behaviour of carbon steel under intermittent oil/water wetting was found to be controlled by the lifetime of the oil film formed on the surface, and a long lifetime or a stabilised oil film can reduce the corrosion rate via acting as a blocking barrier [16]. Surface tension, hydrodynamic condition, and intermolecular interaction play key roles on the stability of the oil film on steel surface [17-19]. Different surface roughness can change the surface tension and intermolecular interaction among oil/water/solid [20]. The investigation of the lifetime of the oil/water films on the surface at various surface conditions helps to reveal the stability of the films under intermittent oil/water wetting with different flow conditions.

To fill the above knowledge gaps, the “alternate wetting cell” designed in our previous research [16] was applied. Based on the statistical analysis of current-time curves measured by potentiostatic polarisation, the relationship between surface roughness and corrosion behaviour of carbon steel under intermittent oil/water wetting at different flow velocities and immersion periods was systematically studied, providing the fundamental insight to the engineer for the safe design and economic pipelines. Additionally, the lifetimes of the oil/water films for different surface conditions were also calculated via the measured current-time curves, the results were linked with equilibrium contact angle and CFD simulation. Finally, the formation and rupture mechanisms of the oil film under static and dynamic flow conditions were proposed, to interpret the corrosion behaviour of carbon steel under intermittent wetting.

2. Experimental procedure

2.1. Material and solution preparation

Test specimens were machined from X65 carbon steel into the cylinder with an outer diameter of 12 mm and a height of 10 mm, which could be mounted to the shaft of the rotating cylinder electrode (RCE) (Figure 1). Table 1 shows the chemical composition of carbon steel. To obtain different surface roughness, the specimens were separately wet-grounded to 60/600 grit silicon carbide paper or abraded with a Kemet 6-micron diamond suspension, followed by rinsing with acetone and distilled water and drying gently with compressed air. To avoid surface oxidation, the experiment was immediately carried out after sample preparation. Besides, the above surface conditions were separately named as 60 Grit, 600 Grit and 6 Micron in the following context.

A mineral oil (viscosity=14.7 mPa·s at 25 °C) and 1 wt. % NaCl solution was used in the present research. Both mediums were bubbled with CO_2 gas for more than 12h in advance, as well as during the entire experiment.

Table 1
Elemental composition of X65 steel (wt.%).

C	P	Si	Cr	Mn	Ni	S	Mo

0.12	0.008	0.18	0.11	1.27	0.07	0.002	0.17
Cu	B	Sn	Ti	Al	Nb	V	Fe
0.12	0.0005	0.008	0.001	0.022	0.054	0.057	Balance

2.2 Intermittent Oil/Water Wetting Experimental Method

Figure 1 presents the schematic of the “alternate wetting cell”, which was designed to simulate intermittent oil/water wetting in our previous research [16]. 250 mL CO_2-saturated brine was added into Beaker1 (500 mL), then 100 mL oil was gently injected, making the working electrode (WE) fully immersed in the oil slug. Beaker 2 (1000 mL) contained CO_2-saturated brine, which was connected to the brine in Beaker 1 by the gear pump and associated tubes. Under the control of Labview, the pump transferred the brine between two beakers and the height of the oil/water interface changed, so the WE was alternately immersed in the oil or the brine slug.

In the present study, the oil immersion period was the same as the water immersion period, 10 and 60 s were separately selected to represent short- and long-term intermittent wetting phenomenon. For rotating speeds of the RCE, 0 and 1000 rpm represent static and dynamic flow conditions respectively, which could be converted to flow velocity of 0 and 0.597 m/s in a 0.1 m-inside-diameter pipe of the Institute for Corrosion and Multiphase Technology (ICMT) [15, 21-23]. Besides, all experiments were conducted at 25°C and each test was repeated at least 3 times.

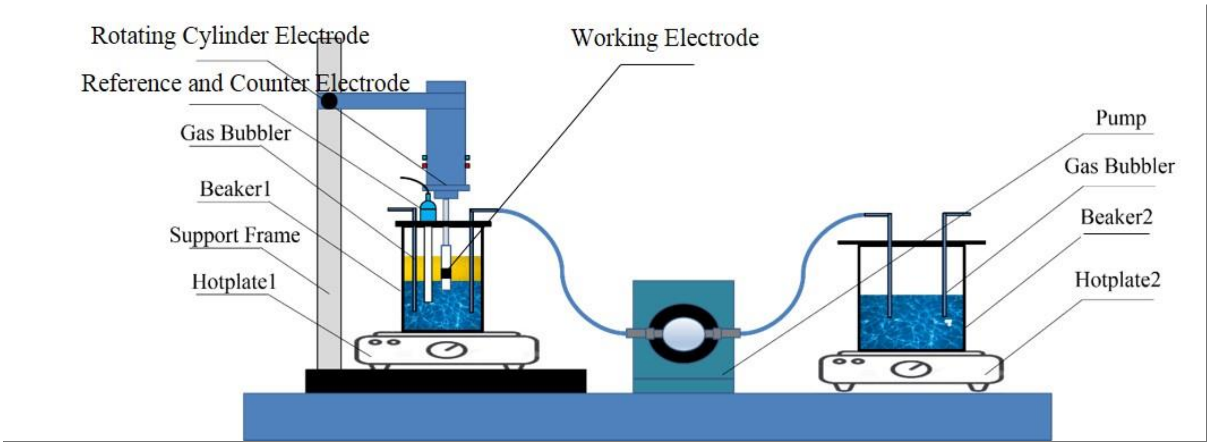

Figure 1. Schematic of the “alternate wetting cell”.

2.3 Electrochemistry measurements

The standard three-electrode cell was applied, as shown in Figure 1. The WE on the RCE shaft was under intermittent wetting, but a saturated Ag/AgCl electrode (reference electrode, RE) and a platinum electrode (counter electrode, CE) were immersed in the CO_2-saturated solution during the whole experiment.

Firstly, the open circuit potential (OCP) of the WE in the CO_2-saturated brine was measured for at least 10 mins until it became stable. Then the potentiostatic polarisation (+10mV vs. OCP) method with 0.1s sampling rate, was used to measure the current of the WE under intermittent oil/water wetting for 1h. The electrochemical measurement was conducted using an Ivium-n-stat.

2.4 Surface analysis

NP_{FLEX} 3D optical non-contact profilometry was employed to determine the surface roughness. 2.0 mm line on the outer surface of the RCE electrode was scanned to assess the roughness. 50× objective was used to scan at 1 × speed. And the surface roughness parameter R_a (arithmetical mean height) and R_{3z} (third maximum peak-to-valley height) were calculated by the software Vision 64. Technical details about roughness parameters can be seen in the Intra, Form Talysurf Operator's Handbook [24].

The oil-in-water contact angle was measured at room temperature using KSV CAM 200 contact angle meter. 2 μL oil was carefully dropped onto the top surface of the cylinder sample in a transparent plexiglass box. Then the CO_2-saturated 1 wt. % NaCl solution was pumped underneath the top surface at 500 mL/min to completely submerge the oil. The whole process was recorded, and the equilibrium oil-in-water contact angle was measured.

2.5 Statistical analysis of current-time curve

Three metrics were proposed to quantitatively study the corrosion behaviour and the wetting behaviour of carbon steel under intermittent wetting phenomenon, based on the statistical analysis of current-time curves measured by the potentiostatic polarisation. For the whole intermittent wetting process, the dissolution mitigation efficiency (DME, η) and the ratio between oil wetting time and water wetting time (θ) were applied. The equation of DME is shown by Eq. (1).

$$DME = \left(1 - \frac{\int_{t_0}^{t_1} I(t)}{\frac{t_1 - t_0}{t_0}\int_0^{t_0} I_0(t)}\right) \times 100\% \quad (1)$$

Where t_0 is the time when the intermittent wetting began, t_1 is the time at the end of the whole electrochemical test, $I_0(t)$ is the measured anodic current of an electrode immersed in the solution at initial 60s, and $I(t)$ represent the anodic current measured under intermittent wetting.

The ratio between oil wetting time and water wetting time (θ) was calculated below:

$$\theta = \frac{t_{oil}}{t_{water}} \tag{2}$$

Where t_{oil} is the sum of time when the current is 0 mA during the whole process of intermittent wetting, and t_{water} represents the sum of time when the current is above 0 mA.

A large DME and θ values represent high efficient corrosion mitigation or a long oil wetting time. The DME and θ are fundamentally determined by the oil/water film caused by the transition between water/oil immersion states. Therefore, the average lifetime of oil/water film during the whole experiment was calculated, which helps to further understand the corrosion process under intermittent wetting. The above data analysis method was conducted by a combined analysis of Excel and MATLAB. More details about the DME and θ can be seen in our previous study [16].

2.6 Computational fluidic dynamics

In this study, computational fluidic dynamics (CFD) simulation of the single-phase flow around the RCE shaft at 1000 rpm in Beaker1 was performed, using ANSYS FLUENT Academic Research R 19.1. The CFD simulation results are used to investigate flow characteristics at the steel surface with different surface roughness.

A 3D geometry of the inner dimensions of the Beaker1 was constructed. The structured hexahedral mesh was generated (ANSYS-ICEM) and y^+ was set 0.1, to accurately reflect near-wall flow characteristics (mesh results seen in Figure S2). Through comparison among different mesh sizes and turbulence models, 359652 cells and the SST k-*w* model with low-Re corrections were chosen (Figure S3 and Table S2). The boundary condition of the shaft of the RCE was set with a rotating speed of 1000 rpm and an equivalent sand-grain roughness model (Details seen in Table S1). The roughness height was equal to the average R_a measured by NP_{FLEX} 3D. Contrarily, boundary conditions of other solid walls of simulated geometry were stationary and without sand-grain roughness. The shear stress and turbulence eddy frequency on the electrode surface were obtained, to quantitatively analyse the effect of surface roughness on near-wall flow characteristics.

The random peaks or valleys of the actual engineering surface have a significant impact on the near-wall flow, which are neglected by the sand-grain roughness model in the 3D simulation. Therefore, a 2D rectangular with a length of 100 μm and a width of 40 μm was built to observe the near-wall flow around the actual surface profile obtained by NP_{FLEX} 3D (Figure S7). More description about the CFD simulation can be seen in Part 3-4 of the *Appendix*.

3. Results

3.1. Surface Analysis

3.1.1 Surface characterization

Figure 2 shows the characterization of surface roughness of RCE samples finished with different sandpapers. As shown in Figure 2(a), the 2D surface profile consisted of arbitrary grooves, the depth of which significantly decreased with finer polishing. The quantitative analysis of surface roughness (Figure 2(b)) indicates that average R_a decreased from 1.775 μm for 60 Grit surface to 0.096 μm for 6 Micron surface, implying that roughness decreased with the particle size of sandpaper. Compared with the average R_a, the average R_{3z} was larger for the same surface condition due to its sensitivity to reflect the high peak or deep valley. The average R_{3z} for 60 Grit surface (6.485 μm) was larger than those of other surface conditions, which is consistent with the 2D surface profile.

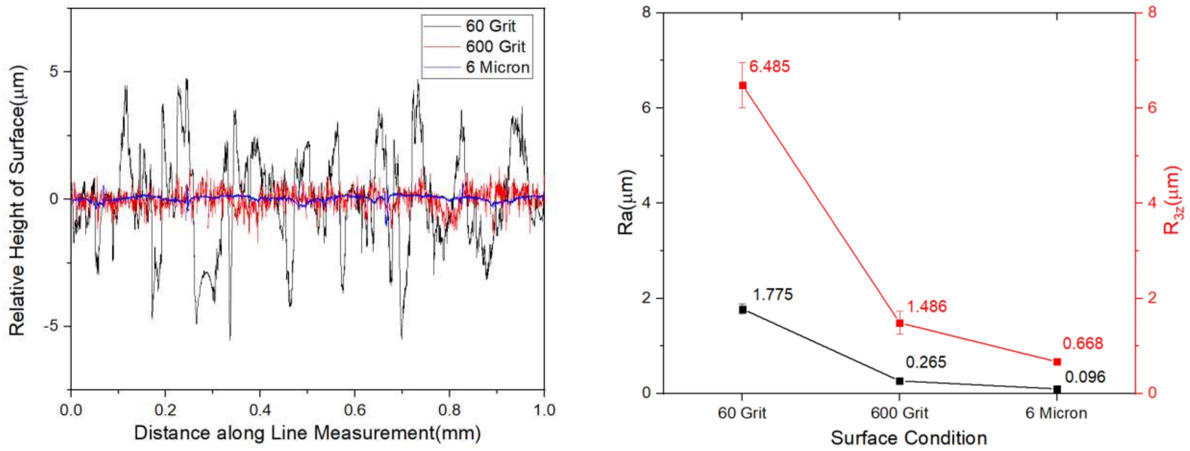

(a) (b)

Figure 2. Characterization of surface roughness of sample obtained by different polishing methods before corrosion. (a) The typical 2D surface profile of the RCE sample, (b) R_a and R_{3z} of the RCE sample.

3.1.2 Equilibrium contact angle for different surface roughness

Figure 3 shows the equilibrium contact angle of the oil-in-water droplet on the carbon steel with different surface conditions. The contact angles on steel surfaces with different roughness were larger than 90°, illustrating that the wettability of all surfaces was water-wet. The contact angle for 60 Grit surface was the smallest (114°), that for 600 Grit surface was the largest (135°). As for the 6 Micron surface, the contact angle was 130°. Therefore, 60 Grit surface was less water-wet and easier to adhere to oil, based on the analysis of contact angle in Part1 of the *Appendix*. Besides, videos of dewetting process of the oil in water (seen in Part2 of the *Appendix*) indicate that the process of changing from oil film to a steady oil droplet on a rougher surface required a longer time, caused by the pinning effect of peak or valley of surface profile [25].

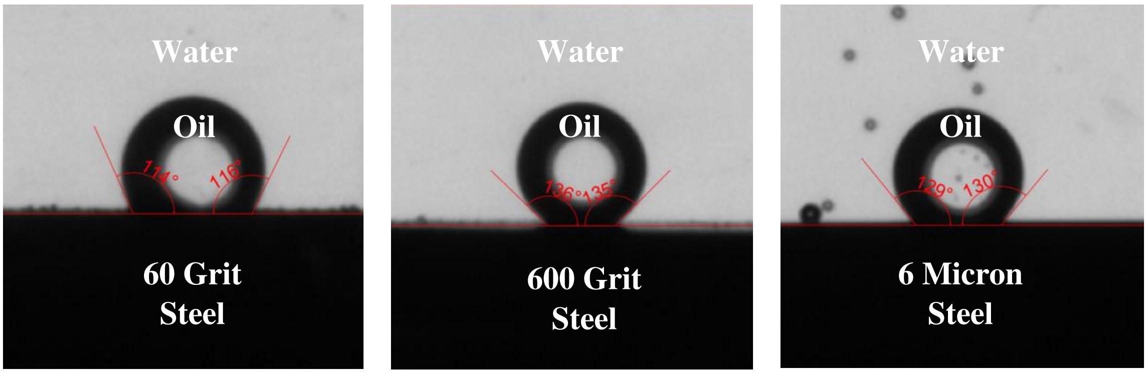

(a) (b) (c)

Figure 3. Oil-in-water contact angle on carbon steel with different surface conditions. (a) 60 Grit (b) 600 Grit (c) 6 Micron.

3.2 Current-time curves of carbon steel with different surface roughness at 0 rpm under intermittent oil/water witting

Figure 4 shows the typical current-time curves of the RCE electrode with different surface roughness at the static condition in an alternate oil/water slug. When the alternate immersion period was 10s, the frequency of the current spike increased with a decrease in surface roughness (Figure 4(a)). As the immersion period increased to the 60s, the current spike frequency for 60 Grit surface was less than those for smooth surface conditions. The current spike represents that the carbon steel is wetted by water and the anodic metal dissolution occurs, therefore, the results suggest that the rough surface can prolong the oil-wetting time under intermittent oil/water wetting at static conditions.

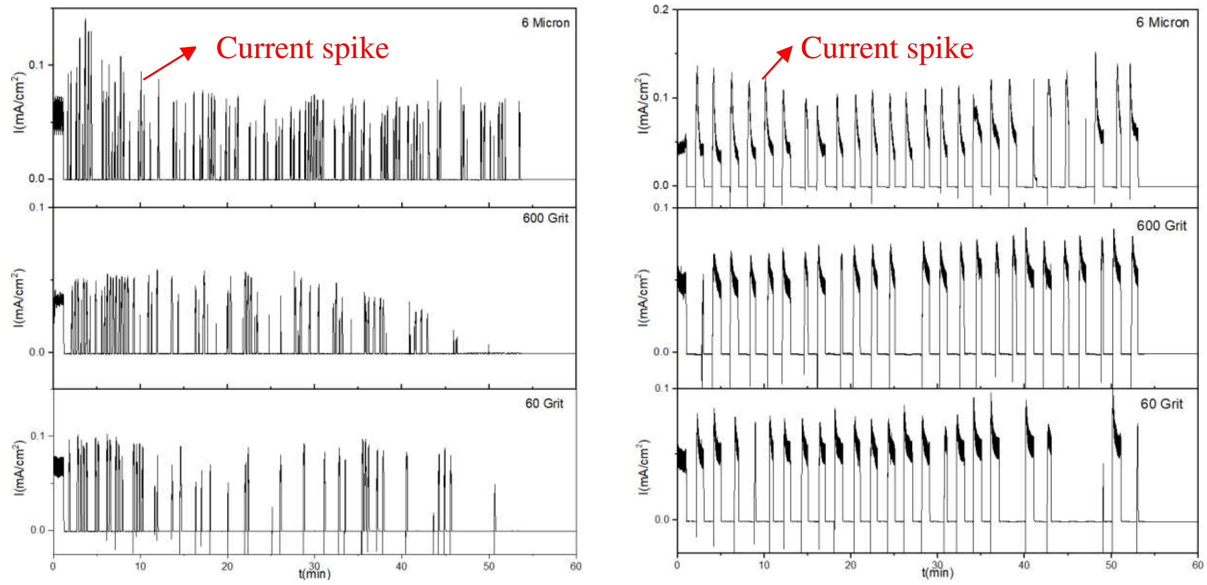

(a) 0 rpm, 10 s (b) 0 rpm, 60 s

Figure 4. Typical current-time curves of the RCE electrode with different surface roughness at the static condition in alternate oil/water slug with different alternate wetting periods of (a) 10 s (b) 60 s.

3.2.1 Statistical analysis of current-time curves of carbon steel at 0 rpm under intermittent oil/water wetting

Figure 5(a) shows the DME and θ of the RCE electrode with different surface roughness under intermittent oil/water wetting at static conditions. When the immersion period was 10 s, DME and θ increased from 88.83% and 7.4 to 91.69% and 11.90 for the increase of surface roughness from 6 Micron to 60 Grit. A large θ for the rough surface represents a long time of oil wetting on the steel surface, which consequently mitigates the corrosion process and increases the DME value.

With the increase of immersion period to 60 s, θ and DME for all surface conditions descended, suggesting a reduction of oil wetting time and corrosion mitigation efficiency. DME for 60 Grit was 70.31%, which was larger than those of smooth surfaces (57.32% and 58.39% for 600 Grit and 6 Micron, respectively). When surface roughness decreased, θ decreased from 2.28 (60 Grit) to 1.52 (600 Grit) and 1.72 (6 Micron). The results indicate that corrosion processes on a rough surface can be efficiently mitigated under intermittent oil/water wetting at a long immersion period of the 60s.

Figure 5(b) illustrates the average lifetime of oil/water films for different surface roughness at static conditions. When the immersion period was 10 s, with the decrease of surface roughness from 6 Micron to 60 Grit, the oil film lifetime slightly increased from 8.05 to 8.70 s, but the water film lifetime decreased from 0.54 to 0.45 s. The results show that the oil film lifetime was longer than the water film lifetime, suggesting that the oil film plays a more important role in corrosion behaviour and the wetting state of carbon steel under intermittent wetting. Besides, the difference between the lifetime of the oil film (range from 8.05 to 8.70 s) and the total immersion period of 10 s was small, implying that the oil film was hard to rupture under intermittent wetting for a short immersion period, consequently leading to a high oil wetting time and corrosion mitigation efficiency in Figure 5(a).

With the rise of the immersion period from 10 to 60 s, the lifetime of the oil film on the surface was doubled, but the lifetime of the water film had no significant influence. The lifetime of the oil film for 60 Grit was the longest (23.63 s), and those for 600 Grit and 6 Micron were 13.15 and 16.30 s, respectively. The difference between the oil film lifetime and the total immersion period of 60 s was large, a large difference suggests that the oil film was easy to rupture under intermittent wetting for an immersion period of 60 s, resulting in a small θ and DME (Figure 5(a)).

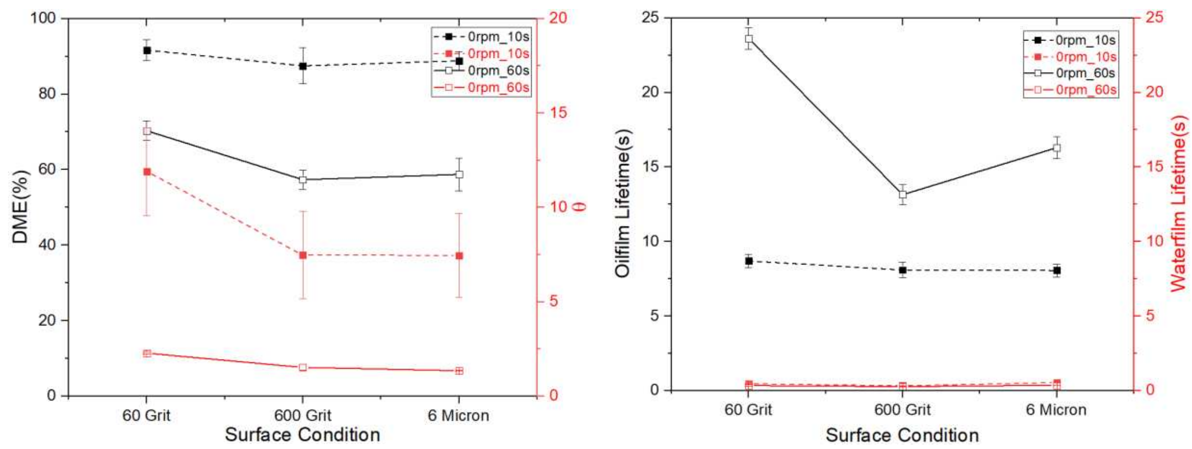

(a) (b)

Figure 5. Statistical analysis of current-time curves of RCE electrode with different surface roughness at the static condition in alternate oil/water slug. (a) DME and Theta (b), the lifetime of the oil/water films.

3.3. Current-time curves of carbon steel with different surface roughness at 1000 rpm under intermittent oil/water wetting

Figure 6 shows typical current-time curves of the RCE electrode with different surface conditions at 1000 rpm during the alternate oil/water slug. Compared with static conditions (Figure 4), the frequency of current spikes at dynamic conditions was increased, implying that the carbon steel is easier to be water-wetting in the dynamic flow. Under the dynamic conditions, the frequency of the current spike had no significant difference for various surface conditions, therefore, a clear relationship between surface roughness and corrosion behaviour of carbon steel at dynamic conditions requires a statistical analysis of current-time curves and the detailed analysis are provided in the following context.

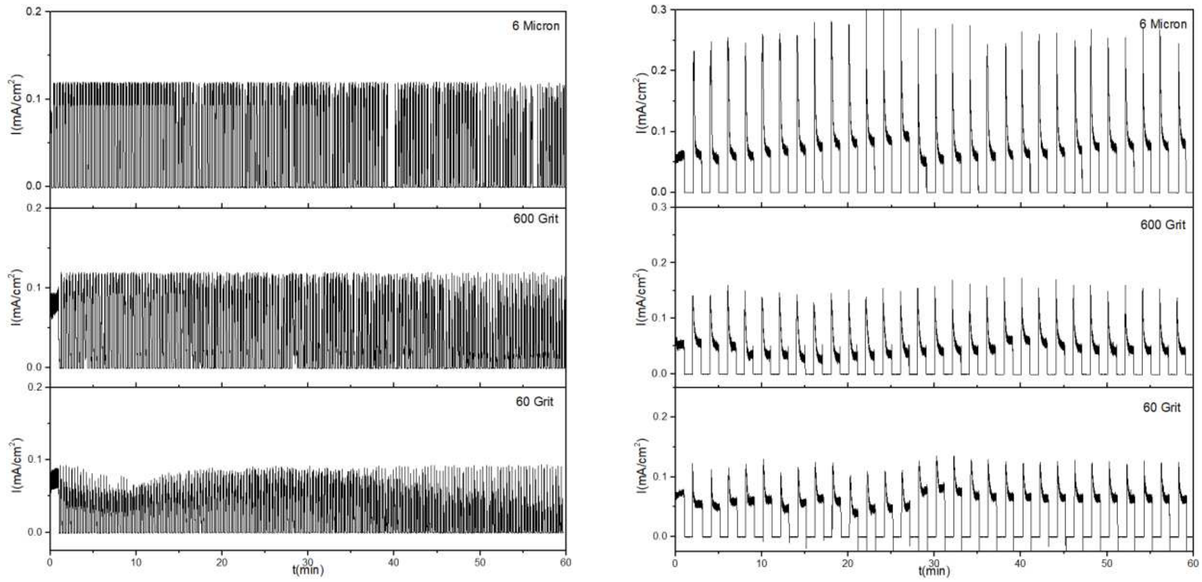

(a) 1000 rpm, 10 s (b) 1000 rpm, 60 s

Figure 6. Typical current-time curves of RCE electrode with different surface roughness at 1000 rpm in alternate oil/water slug with the alternate wetting periods of (a) 10 s (b) 60 s.

3.3.1 Statistical analysis of current-time curves of carbon steel at 1000 rpm under intermittent oil/water wetting

Figure 7(a) shows the DME and θ of the RCE electrode with different surface roughness at dynamic conditions. For immersion periods of 10 and 60 s, the DME and θ for 6 Micron were the largest (67.75%/1.58 and 55.91%/1.10 for 10 s and 60 s, respectively), those for 600 Grit were the smallest (52.84%/0.92 and 48.79%/1.02 for 10 s and 60 s, respectively). The results suggest that corrosion mitigation and oil wetting time increased on a smooth surface, which is contrary to the observation at static conditions (Figure 5(a)). Moreover, θ and DME measured at dynamic conditions were smaller than those at static conditions, suggesting that high flow velocity decreased the oil wetting time and accelerated the corrosion.

Figure 7(b) illustrates the average lifetime of the oil/water films on the RCE electrode with different surface roughness at dynamic conditions. Compared with data measured at static conditions, the lifetime of the oil film for all surface conditions at dynamic conditions was substantially shorter, suggesting that the dynamic flow accelerated the rupture of the oil film on the surface. Moreover, for both immersion periods of 10 and 60 s, the lifetimes of the oil film for 6 Micron (3.41 s and 3.25 s, respectively) were longer than those for rough surfaces (600 Grit and 60 Grit), and the lifetimes of the water film for 6 Micron (0.35 s and 0.28

s, respectively) were the shortest. The results indicate that the oil film on the smooth surface is more stable at the dynamic flow condition, leading to the increase of oil wetting time and corrosion mitigation efficiency (Figure 7(a)).

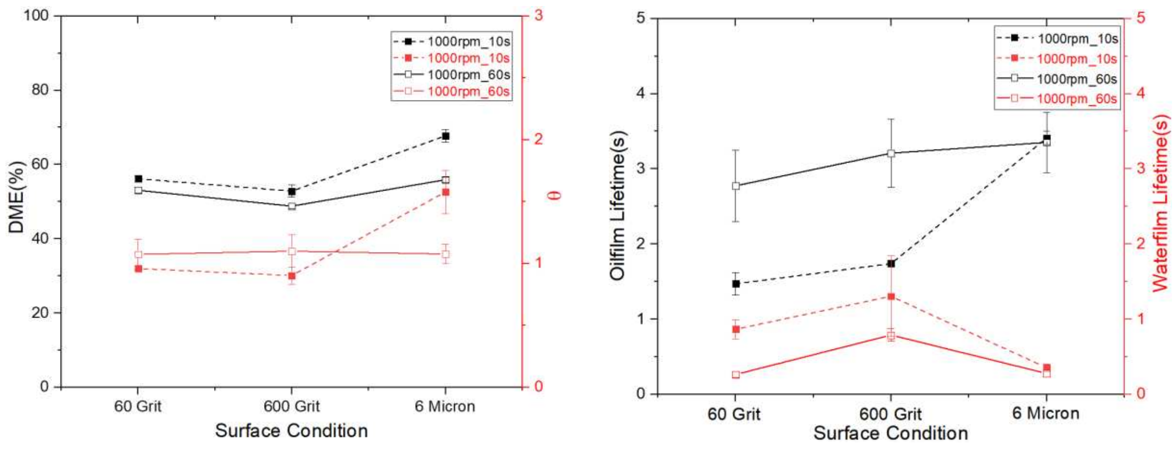

(a) (b)

Figure 7. Statistical analysis of current-time curves of RCE electrode with different surface roughness at the static condition in alternate oil/water slug. (a) DME and Theta (b) Average lifetime of oil and water film.

3.4. CFD simulation

Figure 8 shows the velocity streamlines near the actual profiles for different surface conditions. The turbulence eddies were observed in the cavity for 60 Grit and 600 Grit (Figure 8(a-b)), but no turbulence eddies were observed for 6 Micron (Figure 8(c)). The size of the eddy increased with the surface roughness, suggesting that a rough surface led to high turbulence in the near-wall flow.

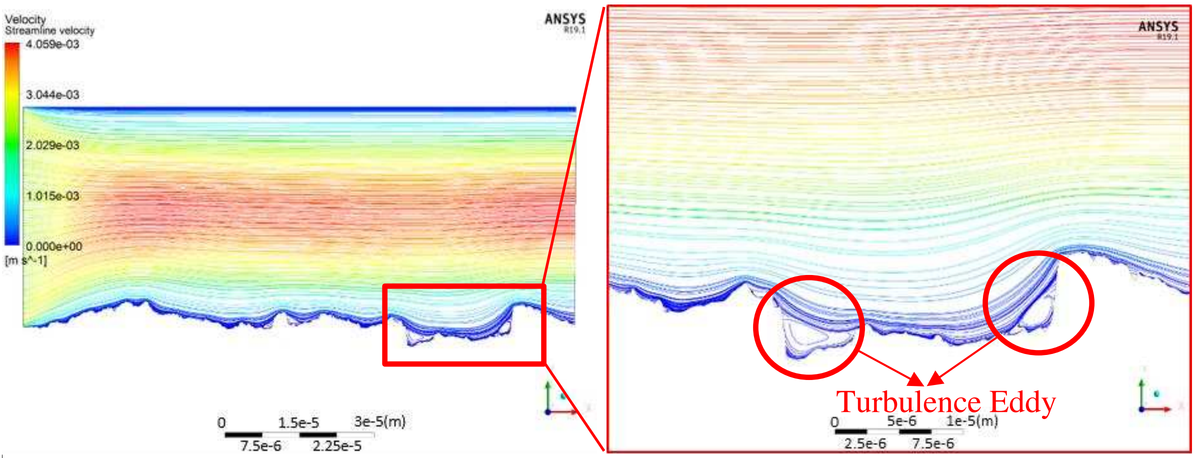

(a)

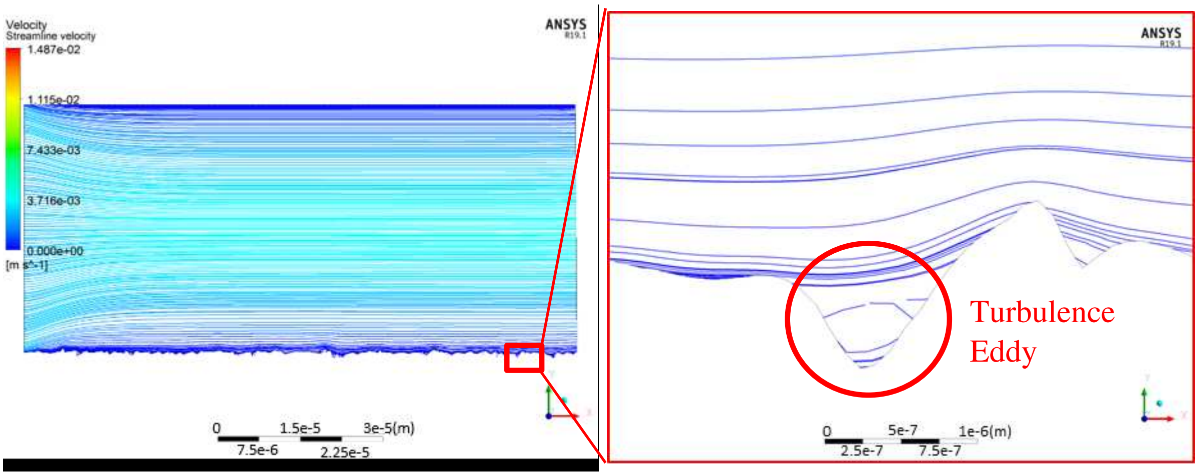

(b)

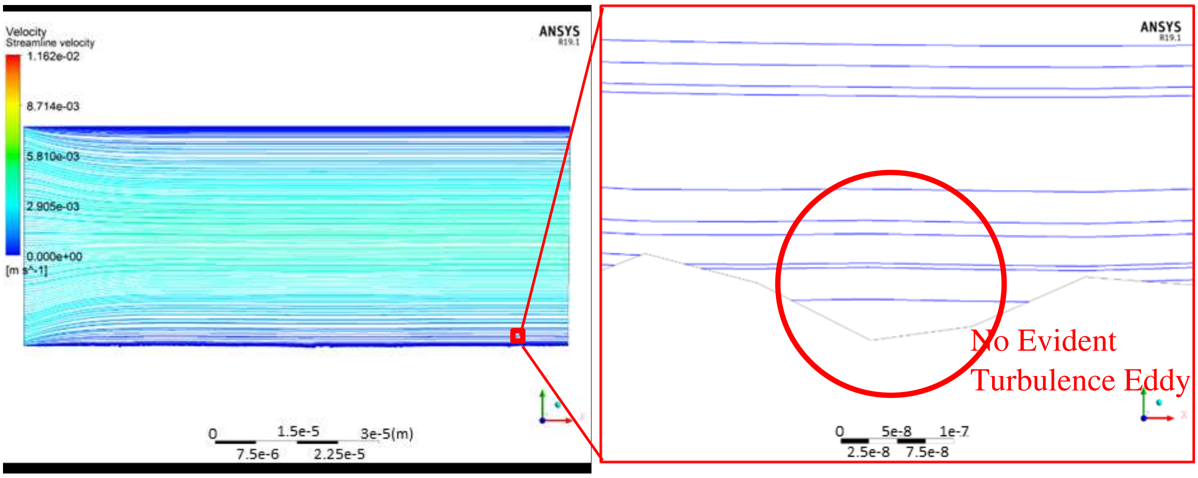

(c)

Figure 8. Velocity streamlines near the profile for different conditions. (a) 60 Grit, (b) 600 Grit, (c) 6 Micron.

Figure 9 reveals the effect of surface roughness on the shear stress and turbulence eddy frequency of the rotating RCE electrode in the oil phase obtained by the CFD simulation. With the decrease of surface roughness from 60 Grit to 6 Micron, shear stress decreased from 6.53 to 6.45 Pa, the turbulence eddy frequency increased from 2.75×10^5 to 2.81×10^5 s^{-1} (Shear stress streamlines and turbulence eddy frequency contours shown in Figure S4-5). The rise of turbulence eddy frequency represents that the size of eddy near the surface decreased with surface roughness, which is in accordance with the above result in Figure 8.

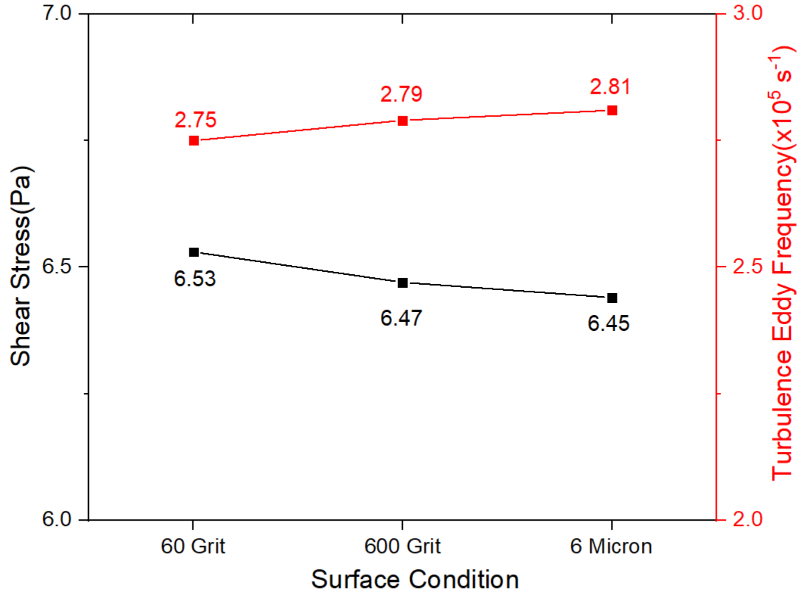

Figure 9. Shear stress and turbulence eddy frequency on the electrode surface with different surface conditions in CFD simulation of RCE in the oil phase.

4. Discussion

4.1 Corrosion mechanism of carbon steel under intermittent oil/water wetting

A schematic diagram of the whole corrosion process of carbon steel under intermittent oil/water wetting is provided in Figure 10. The corrosion process of carbon steel is significantly affected by the wetting states between oil and water. When the carbon steel is covered by the oil (Stage (1-3) in Figure 10), no corrosion occurs and the measured current is 0 mA. For the water wetting, the water becomes saturated with CO_2 via Reactions (3-4);

$$CO_2(g) \leftrightarrow CO_2(l) \tag{3}$$

The hydration of carbonic acid and followed by the dissociation of carbonic acid, bicarbonate ion, and water (Reactions (4-7)).

$$CO_2(l) + H_2O \leftrightarrow H_2CO_3(l) \tag{4}$$

$$H_2CO_3(l) \leftrightarrow H^+(l) + HCO_3^-(l) \tag{5}$$

$$HCO_3^-(l) \leftrightarrow H^+(l) + CO_3^{2-}(l) \tag{6}$$

$$H_2O \leftrightarrow H^+(l) + OH^-(l) \tag{7}$$

The presence of H^+ ions enable the hydrogen evolution (Reaction (8)), which is the dominant cathodic reaction of carbon steel exposed to a low pH CO_2-saturated solution [26-27]. As shown in Reaction (9), the anodic reaction is the dissolution of iron, which is ascertained by the SEM observation of the carbon steel surface after intermittent wetting tests (Figure S8 and S9). It should be noted that the measured anodic current was not significantly influenced by the surface roughness at both static and dynamic conditions (seen in Part 6 in the *Appendix*), despite that the corrosion process in the present research is controlled by mass transfer process [16, 28].

$$2H^{+}+2e^{-}\rightarrow H_2 \tag{8}$$

$$Fe\rightarrow Fe^{2+}+2e^{-} \tag{9}$$

Under intermittent oil/water wetting, the oil immersion period is the same as the water immersion period, as shown in Figure 10. However, the actual calculated oil wetting time is not equal to the water wetting time due to the formation or stability of the oil/water films on the surface caused by the wetting hysteresis under static or dynamic conditions. As shown in Stage (3) in Figure 10, the presence of the oil film on carbon steel can extend 0 mA current segment, suggesting that the oil wetting time is prolonged and the corrosion process can be blocked due to the protective oil film. On the contrary, the presence of water film on the surface extends the anodic current segment (Stage (6) in Figure 10). Furthermore, referring to the previous research about wetting hysteresis theory [29-32], the results in this study indicate that the lifetime of the oil film is longer than that of the water film, which prolongs the total oil wetting time and lowers the corrosion rate.

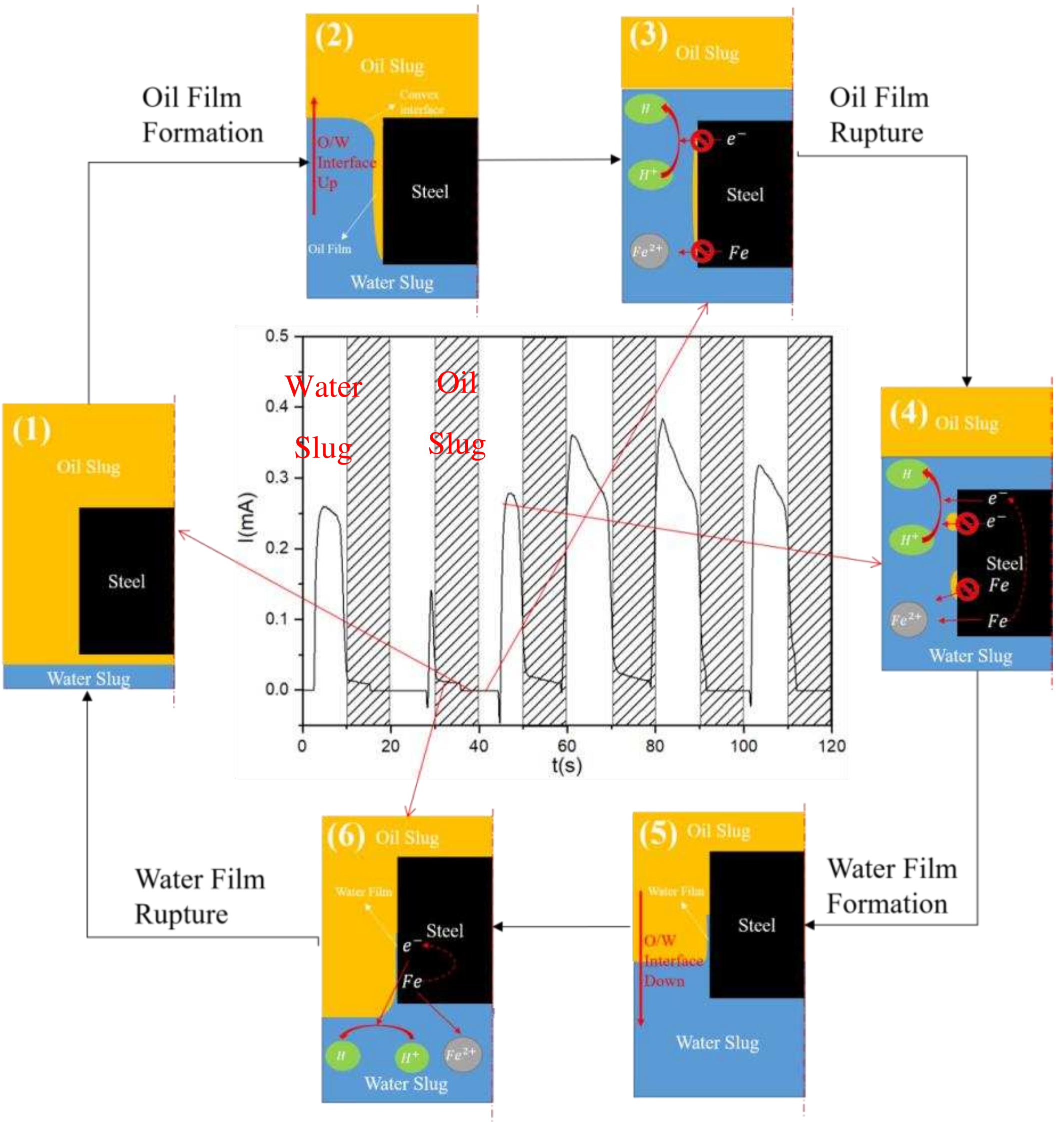

Figure 10. Corrosion mechanism of carbon steel during intermittent oil/water wetting process. The yellow part represents oil, the blue part represents water. And the shadow area represents the oil immersion state, the blank area represents the water immersion state.

4.2 Effect of surface roughness on corrosion behaviour of carbon steel at static conditions under intermittent oil/water wetting

The data in Section 3.2 demonstrates that metal dissolution processes for a rough surface condition were mitigated under intermittent wetting at static conditions for the immersion periods of 10 and 60 s.

According to the corrosion mechanism described in Section 4.1, the corrosion behaviour of carbon steel with different surface conditions under intermittent wetting at static conditions is determined by the formation and rupture of the oil film. As shown in the formation process of the oil film (Figure 11(a)), the thickness of the oil film is proportional to the Capillary number (Ca) to the power 2/3 based on the Landau-Levich model [33]. The Ca is calculated as below:

$$Ca = \frac{\mu V}{\gamma} \qquad (10)$$

where μ is the dynamic viscosity of the liquid, V is the contact line velocity and γ is the surface tension between oil and water. The observation in previous research [34-35] indicated that the thickness of the oil film increased with surface roughness, and consequently a stable oil film formed on the surface.

The rupture of the oil film in water at the static conditions is governed by the force balance among gravity, pressure, viscous force, and surface tension (Figure 11(b)) based on the theoretical studies about the stability of the films [36-37]. To simplify the model, the Bond number (Bo, shown in Equation (11)) and Ca, which separately reflect the importance of gravitational force and viscous drag force compared to surface tension, are calculated.

$$Bo = \frac{\Delta\rho g L^2}{\gamma} \qquad (11)$$

where $\Delta\rho$ is the density difference between the two phases, g is the acceleration due to gravity, L is the characteristic length that is the oil film thickness in the present research, and γ is the surface tension between oil and water. The thickness of the oil film is 0.1 mm for 600 Grit according to the observation, Bo is 2.275×10^{-4}. Besides, the contact line velocity is 0 m/s in the initial stage, so the calculated Ca is 0. In the Bo and Ca are << 1 condition, surface tension plays an important role in the stability of the oil film on the surface.

As shown in Figure 11(b), the surface tension of the oil film can be decomposed into γ_{so} (steel-oil surface tension) and γ_{wo} (water-oil surface tension). The γ_{wo} is constant for the present oil/water system, therefore, the γ_{so} determines the stability of the oil film in water. A large γ_{so} represents that the steel surface is less adhesive to the oil film, the film is consequently easier to breakdown into the oil droplets as shown in Figure 11(c). As described in Results 3.1, the contact angle of oil-in-water on carbon steel with different surface conditions suggests that γ_{so} for 60 Grit is the smallest, and the oil film is stable. Therefore, the oil wetting time and corrosion mitigation efficiency for 60 Grit are the largest at the static condition, as demonstrated in Figure 5.

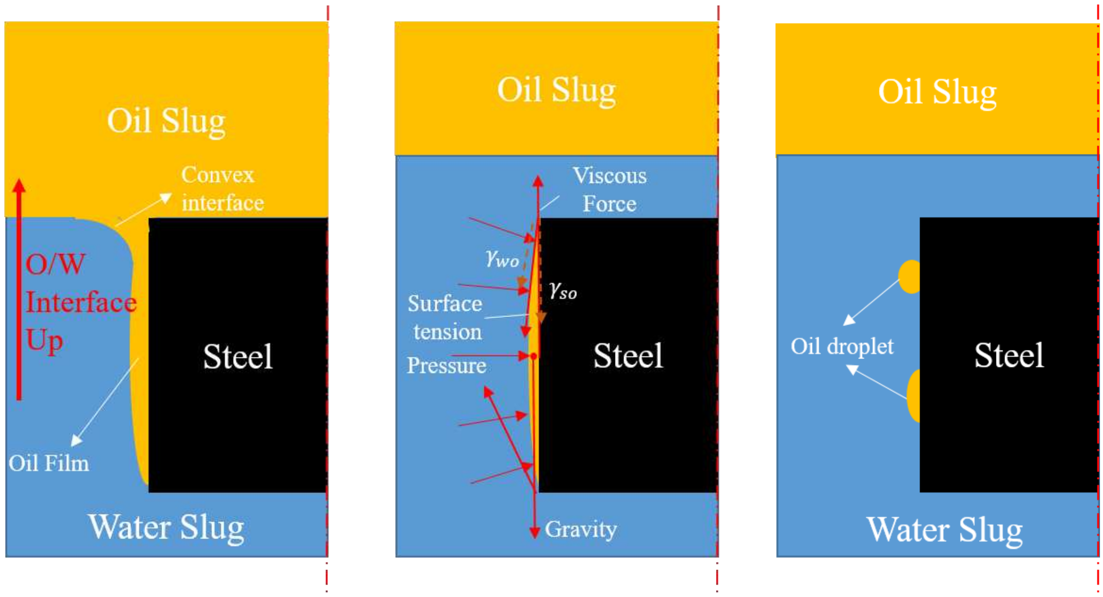

(a) (b) (c)

Figure 11. Schematic of the formation and rupture of the oil film in water at static conditions. (a) Formation of the oil film in water during intermittent wetting (b) Force analysis of the oil film in water (c) Rupture of the oil film in water. The yellow part represents oil, the blue part represents water.

4.3 Effect of surface roughness on corrosion behaviour of carbon steel at dynamic conditions under intermittent oil/water wetting

The data in Section 3.3 demonstrates that at dynamic conditions, the corrosion process at the material interface (smooth surface condition) was mitigated efficiently for both short and long immersion periods under intermittent wetting, which is different from the results found at static conditions.

Compared with static conditions, the reduction in the oil film lifetime and the area of the un-corroded island can be recorded via a combination of electrochemical measurements (Figure 7(b)) and the SEM images as shown in Part 5 in the *Appendix*, the results suggest that the shear stress and turbulence eddy can decrease the stability of the oil film on the surface at the dynamic conditions [38-39]. In the oil film formation process, the near-wall flow around the RCE electrode is continuous in bulk oil and the oil film (Figure 12(a)), based on the visualisation of the Landau-Levich flow field [40]. The stability of the film is determined by the shear stress between the oil film and bulk solution (Figure 12(b and c)). As shown in the magnified view of near-wall interface (Figure 12(b)), small shear stress and turbulence eddy size on a smooth surface (seen in CFD simulation results in Figure 8-9) can contribute to a thick and stable oil film. Therefore, the lifetime of the oil film for the smooth surface is long, and the oil wetting time and corrosion mitigation efficiency increases as demonstrated in Figure 7.

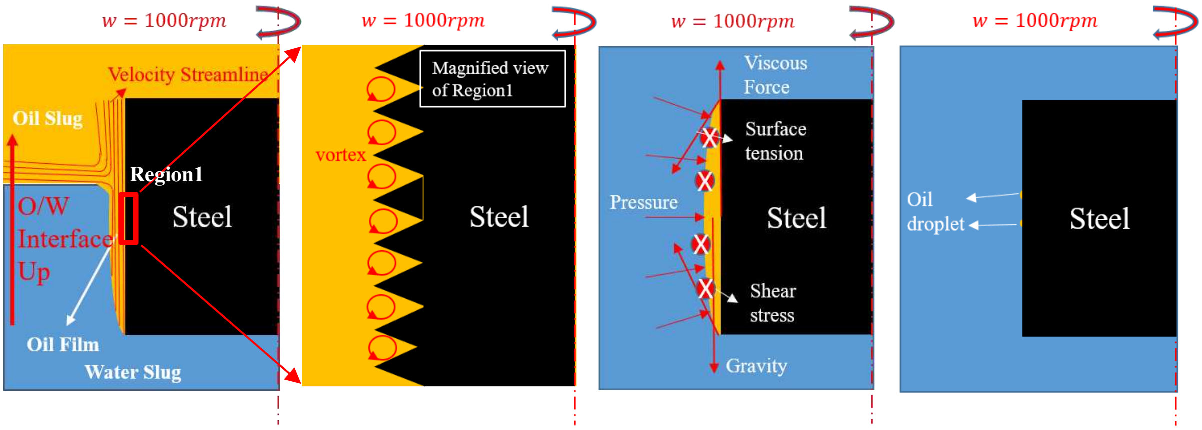

(a) (b) (c) (d)

Figure 12. Schematic of the formation and rupture of oil film at dynamic conditions. (a) Formation of the oil film during the transition from oil immersion to water immersion (b) Magnified view of near-wall turbulent vortex in Region1 (c) Force analysis of the oil film in water (d) Rupture of the oil film in water. The yellow part represents oil, the blue part represents water.

5. Conclusion

The effect of surface roughness on corrosion behaviour of carbon steel under intermittent oil/water wetting at the rotating speeds of 0/1000 rpm and alternate oil/water immersion periods of 10/60 s were systematically investigated by a new-modified “alternate wetting cell”. From this study, the following conclusion can be made:

1. When the rotating speed was 0 rpm, the DME for 60 Grit was the largest than that for other smooth surfaces at the immersion period of 10 and 60 s, implying that a rough surface contributes to the corrosion mitigation under intermittent oil/water wetting.
2. At the static conditions, surface tension is the key factor for the stability of oil film on the surface, and the reduction in corrosion process can be contributed to the small surface tension under intermittent wetting, especially for a long immersion period of the 60s.
3. When the rotating speed was 1000 rpm, the DME for 6 Micron was the largest for both short and long immersion periods (10 s and 60 s), illustrating that a smooth surface can mitigate corrosion efficiently.
4. At the dynamic conditions, the shear stress and turbulence eddy determine the stability of oil film and corrosion behaviour under intermittent wetting. A smooth surface can decrease the shear stress and size of turbulence eddy,

which consequently increases the lifetime of the oil film on the surface and mitigates the corrosion process.

Acknowledgments

This work was supported by the Shandong Provincial Natural Science Foundation (Grant No. ZR202102190003).

Data Availability

The processed data required to reproduce these findings cannot be shared at this time as the data also forms part of an ongoing study.

CRediT authorship contribution statement:

Wenlong Ma: Conceptualization, Methodology, Software, Formal analysis, Investigation, Data Curation, Simulation, Writing – Original Draft, Writing – Review & Editing, Visualization

Hanxiang Wang: Conceptualization, Writing – Review & Editing, Supervision

Yongxing Wang: Simulation, Writing – Review & Editing

Anne Neville: Methodology, Supervision, Funding acquisition

Yong Hua: Conceptualization, Methodology, Resources, Writing – Review & Editing, Supervision

6. Reference:

1. Koch, Gerhardus H., Michiel PH Brongers, Neil G. Thompson, Y. Paul Virmani, and Joe H. Payer. Corrosion cost and preventive strategies in the United States. No. FHWA-RD-01-156,. 2002.

2. Farshad, Fred F., and Herman H. Rieke. "Surface roughness design values for modern pipes." SPE Drilling & Completion 21, no. 03 (2006): 212-215.

3. Li, W., and D. Y. Li. "Influence of surface morphology on corrosion and electronic behavior." Acta materialia 54, no. 2 (2006): 445-452.

4. Lee, Sang Mok, Wan Gyu Lee, Yeong Ho Kim, and Ho Jang. "Surface roughness and the corrosion resistance of 21Cr ferritic stainless steel." Corrosion Science 63 (2012): 404-409.

5. Kim, Su Kyeng, In Jun Park, Dong Young Lee, and Jung Gu Kim. "Influence of surface roughness on the electrochemical behavior of carbon steel." Journal of Applied Electrochemistry 43, no. 5 (2013): 507-514.

6. Li, Yuan, and Y. Frank Cheng. "Effect of surface finishing on early-stage corrosion of a carbon steel studied by electrochemical and atomic force microscope characterizations." Applied Surface Science 366 (2016): 95-103.

7. Zhang, Huan-huan, Xiaolu Pang, and Kewei Gao. "Effect of surface roughness on the performance of thioureido imidozaline inhibitor in CO_2-saturated brine." Corrosion Science 157 (2019): 189-204.

8. Evgeny, Barmatov, Trevor Hughes, and Dmitry Eskin. "Effect of surface roughness on corrosion behaviour of low carbon steel in inhibited 4 M hydrochloric acid under laminar and turbulent flow conditions." Corrosion Science 103 (2016): 196-205.

9. Al-Khateeb, Mohammed, Richard Barker, Anne Neville, and Harvey Thompson. "An experimental and theoretical investigation of the influence of surface roughness on corrosion in CO_2 environments." Journal of Corrosion Science and Engineering 20 (2018).

10. Alim, Nor Asma Rusni Ab, and Nor Asma Rusni. "A study on the effect of surface finish on corrosion of carbon steel in CO_2 environment." (2008).

11. Levich, Veniamin G., and Charles W. Tobias. "Physicochemical hydrodynamics." Journal of The Electrochemical Society 110, no. 11 (1963): 251C.

12. Dawson, David A., and Olev Trass. "Mass transfer at rough surfaces." International Journal of Heat and Mass Transfer 15, no. 7 (1972): 1317-1336.

13. Schmitt, Guenter, Gilda Karbasi, Srdjan Nešic, Brian Kinsella, Bruce Brown, and Rudolf Hausler. "Pitting in the water/hydrocarbon boundary region of pipelines-Effect of corrosion inhibitors." In CORROSION 2013. OnePetro, 2013.

14. Wang, Zi Ming, Qing Yu Lun, Jian Wang, Xia Han, Wei Zhu, Jian Zhang, and Guang-Ling Song. "Corrosion mitigation behavior of an alternately wetted steel electrode in oil/water media." Corrosion Science 152 (2019): 140-152.

15. Tang, Xuanping. "Effect of surface state on water wetting and carbon dioxide corrosion in oil-water two-phase flow." PhD diss., Ohio University, 2011.

16. Ma, Wen Long, Han Xiang Wang, Richard Barker, Nikil Kapur, Yong Hua, and Anne Neville. "Corrosion behaviour of X65 carbon steel under the intermittent oil/water wetting: A synergic effect of flow velocity and alternate immersion period." Corrosion Science (2021): 109507.

17. Ajaev, Vladimir S. "Instability and rupture of thin liquid films on solid substrates." Interfacial Phenomena and Heat Transfer 1, no. 1 (2013).

18. Craster, Richard V., and Omar K. Matar. "Dynamics and stability of thin liquid films." Reviews of modern physics 81, no. 3 (2009): 1131.

19. Yarin, Alexander L., Alexander Oron, and Philip Rosenau. "Capillary instability of thin liquid film on a cylinder." Physics of Fluids A: Fluid Dynamics 5, no. 1 (1993): 91-98.

20. Cai, J. Y., Srdjan Nesic, Chong Li, Xuanping Tang, Francois Ayello, Ivan Cruz, and Jamal Khamis. "Experimental studies of water wetting in large diameter horizontal oil-water pipe flows." In SPE Annual Technical Conference and Exhibition. Society of Petroleum Engineers, 2005.

21. Kee, Kok Eng. "A study of flow patterns and surface wetting in gas-oil-water flow." PhD diss., Ohio University, 2014.

22. Papavinasam, S., A. Doiron, T. Panneerselvam, and R. W. Revie. "Effect of hydrocarbons on the internal corrosion of oil and gas pipelines." Corrosion 63, no. 7 (2007): 704-712.

23. Li, Chong, Xuanping Tang, Francois Ayello, Jiyong Cai, Srdjan Nesic, C. Ivan T. Cruz, and Jamal N. Al-Khamis. "Experimental study on water wetting and CO_2 corrosion in oil-water two-phase flow." NACE Corrosion 6595 (2006).

24. Intra, Form Talysurf. "Operator’s Handbook." (2002).

25. Quéré, David. "Wetting and roughness." Annu. Rev. Mater. Res. 38 (2008): 71-99.

26. Nešić, Srdjan. "Key issues related to modelling of internal corrosion of oil and gas pipelines–A review." Corrosion science 49, no. 12 (2007): 4308-4338.

27. Zhang, G. A., and Y. F. Cheng. "Electrochemical characterization and computational fluid dynamics simulation of flow-accelerated corrosion of X65 steel in a CO_2-saturated oilfield formation water." Corrosion Science 52, no. 8 (2010): 2716-2724.

28. Ortega-Toledo, D. M., J. G. Gonzalez-Rodriguez, M. Casales, L. Martinez, and A. Martinez-Villafañe. "CO_2 corrosion inhibition of X-120 pipeline steel by a modified imidazoline under flow conditions." Corrosion Science 53, no. 11 (2011): 3780-3787.

29. Al-Shareef, Amer, Partho Neogi, and Baojun Bai. "Force based dynamic contact angles and wetting kinetics on a Wilhelmy plate." Chemical Engineering Science 99 (2013): 113-117.

30. Quéré, David. "Fluid coating on a fiber." Annual Review of Fluid Mechanics 31, no. 1 (1999): 347-384.

31. Maleki, M., M. Reyssat, F. Restagno, D. Quéré, and Christophe Clanet. "Landau–levich menisci." Journal of colloid and interface science 354, no. 1 (2011): 359-363.

32. Snoeijer, Jacco H., and Bruno Andreotti. "Moving contact lines: scales, regimes, and dynamical transitions." Annual review of fluid mechanics 45 (2013): 269-292. 33. Rio, Emmanuelle, and François Boulogne. "Withdrawing a solid from a bath: How much liquid is coated?." Advances in colloid and interface science 247 (2017): 100-114.

34. Champougny, Lorène, Emmanuelle Rio, Frédéric Restagno, and Benoit Scheid. "The break-up of free films pulled out of a pure liquid bath." Journal of fluid mechanics 811 (2017): 499-524.

35. Krechetnikov, R., and G. M. Homsy. "Experimental study of substrate roughness and surfactant effects on the Landau-Levich law." Physics of Fluids 17, no. 10 (2005): 102108.

36. Takagi, Daisuke, and Herbert E. Huppert. "Flow and instability of thin films on a cylinder and sphere." Journal of Fluid Mechanics 647 (2010): 221.

37. Yarin, Alexander L., Alexander Oron, and Philip Rosenau. "Capillary instability of thin liquid film on a cylinder." Physics of Fluids A: Fluid Dynamics 5, no. 1 (1993): 91-98.

38. Hu, Howard H., and Daniel D. Joseph. "Lubricated pipelining: stability of core-annular flow. Part 2." Journal of fluid mechanics 205 (1989): 359-396.39. Yan, Jenn-Feng, A. Eduardo Sáez, and Christine S. Grant. "Removal of oil films from stainless steel tubes." AIChE journal 43, no. 1 (1997): 251-259.

40. Mayer, H.C. and Krechetnikov, R. "Landau-Levich flow visualization: Revealing the flow topology responsible for the film thickening phenomena." Physics of Fluids 24, no. 5 (2012): 052103.